# Formation of Bioinorganic Complexes by the Corrosive Adsorption of (*S*)-Proline on Ni/Au(111)

*Riho T. Seljamäe-Green†, Grant J. Simpson†, Federico Grillo†, John Greenwood†§, Stephen M. Francis†, Renald Schaub†, Jerome E. Gano†, Herbert A. Früchtl†,Paolo Lacovig‡ and Christopher J. Baddeley†**

†EaStCHEM School of Chemistry, University of St Andrews, St Andrews, Fife, KY16 9ST, UK

‡Elettra - Sincrotrone Trieste S.C.p.A., Strada Statale 14 Km 163.5, I-34149 Trieste, Italy.

KEYWORDS: Nickel, STM, XPS, HREELS, chiral, amino acid, proline.

ABSTRACT: Nickel nanoparticles modified by the adsorption of chiral amino acids are known to be effective enantioselective heterogeneous catalysts. The leaching of nickel by amino acids has a number of potential effects including the induction of chirality in the nickel atoms left behind in the nanoparticle and the creation of catalytically active nickel complexes. The adsorption of (*S*)-proline onto Au(111) precovered by two dimensional nickel nanoclusters was investigated by scanning tunnelling microscopy, X-ray photoelectron spectroscopy and high resolution electron energy loss spectroscopy. Adsorption of (*S*)-proline at 300 K resulted in the corrosion of the nickel clusters, the oxidation of the leached nickel and the on-surface formation of bioinorganic complexes, which are concluded to contain three prolinate species in an

octahedral arrangement around the central Ni ion. Two distinguishable forms of nickel prolinate complexes were identified. One form self-assembles into 1-D chains and the other form gives rise to porous 2-D islands. Octahedral complexes of the type $M(AB)_3$ are intrinsically chiral resulting in two pairs of enantiomers. The mirror symmetry of each pair of enantiomers is broken when, as in this study, the bidentate ligand itself possesses a chiral center. DFT calculations are used to examine the relative energies of each $Ni(prolinate)_3$ complex as isolated gas phase species and isolated adsorbed species.

## INTRODUCTION

Amino acids are key building blocks in the formation of peptide linkages and proteins in biological organisms. All the proteinogenic amino acids, except glycine, are chiral having the possibility of existing in two mirror equivalent enantiomeric forms. For reasons not yet clearly understood, α-amino acids in living organisms on Earth exist exclusively in the L- enantiomeric form with the exception of a minority of amino acids in bacterial cell walls.[1] In addition to their potential role in the origin of biomolecular homochirality,[2-4] adsorbed amino acids have applications as biosensors[5] and as chiral modifiers in enantioselective catalysis.[6] The interest in amino acid interactions with surfaces has motivated many recent surface science investigations.[7-20]

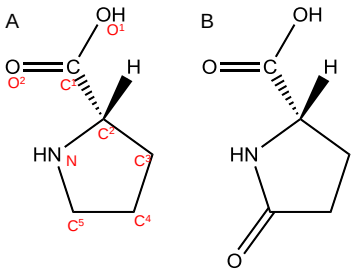


**Figure 1.** Molecular structure of (*S*)-proline (A) and (*S*)-pyroglutamic acid (B)

A fascinating feature of many amino acids is their ability to corrode and restructure metal surfaces. Most strikingly, Zhao showed that the adsorption of lysine onto Cu(001) resulted in the restructuring of Cu steps and chiral faceting of the Cu surface.[21] Despite the adsorption of amino acids being relatively weak on Au surfaces, lysine has been shown to induce restructuring of Au steps to produce Au nanofingers on the Au(111) surface.[22] Dramatic etching effects have been observed following the adsorption of glutamic acid onto Au(111) surfaces pre-covered in 2-D nanoclusters of Ni.[18] The adsorption of glutamic acid results in the removal of Ni from the metallic clusters and the formation of 1-D chains which were shown to be composed of nickel pyroglutamate units. Pyroglutamic acid (Figure 1B) contains a five membered pyrrolidone ring and is formed by the internal cyclisation of glutamic acid. Similar behavior was reported following the adsorption of lysine onto Ni clusters on Au(111).[23] In each of these cases, it was proposed that metallic Ni is oxidized to $Ni^{2+}$ by the interaction with the amino acid.[18,23] The understanding of interactions between divalent cations of transition metals is of importance not only in understanding the functioning of biological macromolecules such as enzymes and proteins, but also in the formation of peptides from amino acids.[24] From the viewpoint of enantioselective catalysis, the formation of chiral arrangements of metal atoms or chiral organometallic complexes following corrosion by a chiral amino acid could provide active sites for enantioselective surface chemistry. On an achiral surface, the adsorption of a planar pro-chiral reagent has an equal probability of occurring *via* either enantiotopic face. The docking of prochiral reagents could reasonably be expected to be skewed in favor of one enantiotopic face by the surface chirality induced by amino acid adsorption. For example, in the glutamic acid on Ni/Au(111) system, the 1-D chains of pyroglutamate were shown to supply docking sites for the prochiral reagent, methyl acetoacetate (MAA), and induce ordered arrangements of MAA in the

regions separating the chains of metal organic structures.[25] Trant and Baddeley[25] proposed that the 1-D chains exhibited chiral recognition and possibly also chiral amplification effects which could be potentially exploitable in the rational design of enantioselective heterogeneous catalysts.

In this study, we chose to investigate the structurally similar amino acid (*S*)-proline (Figure 1A) in order to probe the effect of removing the carbonyl group from the pyrrolidone ring on the ability of proline to form metal-organic structures. (*S*)-Proline is of additional interest as it is used widely in chiral organic synthesis, for example in the hydrogenation of α,β-unsaturated ketones[26] such as isophorone and in the hydrogenation of substituted aromatic compounds, such as unsymmetrically substituted aromatics.[27] The adsorption of proline has been reported on Cu(110),[10,11] $TiO_2$(110),[28,29] Pd(111),[8] and Au(111)[30] surfaces. Proline adsorbs on Cu(110) as an anionic prolinate species in the $\mu_3$ form (*i.e.* both oxygens of the carboxylate functionality and the nitrogen of the pyrrolidine ring are bonded to surface Cu atoms). A (4×2) structure is formed that is stable up to 450 K when decomposition occurs. Both the anionic and the zwitterionic forms are detected on $TiO_2$(110) with the anionic form being the dominant species.[28,29] The zwitterionic form becomes less stable with increasing temperature and desorbs at 600 K, though the anionic form persists. On Pd(111), proline adsorbs in either the neutral or the zwitterionic form. Adsorption below 300 K results in a mixture whilst adsorption at 300 K results exclusively in zwitterionic proline.[8] Decomposition of adsorbed proline begins at 390 K.[8] On Au(111), both the zwitterionic and neutral forms of proline are detected. At 300 K, in the submonolayer regime, these species form a 2-D gas which desorbs following annealing to 370 K.[30]

In this work, the adsorption of proline has been studied on Ni/Au(111) at submonolayer coverages of Ni using scanning tunnelling microscopy (STM); high resolution electron energy

loss spectroscopy (HREELS) and X-ray photoelectron spectroscopy (XPS). Proline is shown to corrosively oxidize the 2D Ni nanoclusters forming a number of ordered molecular arrangements. The composition and structure of these arrangements are identified and discussed.

## EXPERIMENTAL SECTION

### *Low Temperature Scanning Tunneling Microscopy* (LT-STM)

Low Temperature STM experiments were performed in an ultrahigh vacuum (UHV) surface analysis system with a base pressure below $1 \times 10^{-10}$ mbar consisting of a preparation chamber allowing for standard sample preparation and a microscope chamber housing a CreaTec low-temperature STM. STM was performed at 77 K in constant-current mode utilizing homemade PtIr tips.

Ni deposition was achieved by passing a current directly through a high purity Ni filament and the Ni deposition rate was calibrated *via* STM by monitoring the size of the 2-D Ni clusters that nucleate into elbows of the herringbone reconstruction.[31]

### *High resolution electron energy loss spectroscopy (HREELS)*

HREELS measurements were carried out using a VSW HIB 1000 double pass spectrometer mounted on a UHV chamber working with a base pressure better than $2 \times 10^{-10}$ mbar, in the specular geometry ($\theta_i = \theta_f = 45°$), with a primary beam energy of 4 eV and a typical elastic peak resolution of *ca*. 50 $cm^{-1}$ (6.2 meV FWHM). Spectra were normalized to the elastic peak intensity. Sample preparation was carried out in an adjacent UHV preparation chamber with a base pressure better than $5 \times 10^{-10}$ mbar, allowing fast transfer between the two chambers and preserving a contamination free environment for HREEL measurements. A maximum likelihood based resolution enhancement method was used to recover the spectra from the instrumental

broadening.[32,33] Ni deposition was achieved with the same calibrated doser as used on the STM chamber as the doser-crystal positions were very similar in both chambers.

*X-ray Photoelectron Spectroscopy (XPS)*

The photoemission studies were performed at the SuperESCA beamline[34,35] of the Elettra third generation synchrotron radiation source in Trieste, Italy. The experimental chamber was equipped with a Phoibos hemispherical energy analyzer (SPECS GmbH) with a homemade delay-line detector[36] and has a background pressure of about $2 \times 10^{-10}$ mbar. Core level spectra were recorded with the sample at room temperature and at a photon energy of 970 eV (Ni $2p_{3/2}$), 320 eV (Au 4f), 400 eV (C 1s) 500 eV (N 1s), or 650 eV (O 1s), with an overall energy resolution of better than 100-250 meV. Core level spectra binding energies were referenced to the Fermi level. XP spectra were used to verify surface cleanliness. Ni deposition was achieved using an e-beam evaporator and calibrated to the attenuation of the Au 4f peak.

In each chamber, the Au(111) crystal was cleaned by repeated cycles of $Ar^+$ sputtering at 300 K and whilst cooling from 575 K. After each sputter the surface was annealed at 825-875 K for ~10 min. 0.15 monolayers (ML) of Ni was deposited on the reconstructed surface.[37] Ni coverage is estimated from the STM images by measuring the percentage coverage of the Au substrate by Ni clusters. The sample was then exposed to (*S*)-proline (SigmaAldrich, ≤99.5%) *via* sublimation from a solid doser in the same manner as has been previously reported.[30]

The core level XP spectra were fitted using the CasaXPS commercial fitting package using a Shirley type background and a Gaussian (70%)-Lorentzian (30%) shape function for each emission.

*DFT Calculations*

The complex was simulated with ORCA using the PBE functional[38] with Grimme's D3 dispersion correction and Becke-Johnson damping (D3BJ).[39] The Ahlrichs def2-TZVP basis set[40] was used with f functions removed. Vibrational spectra were calculated using the same program and method.

Periodic DFT calculations were carried out using the VASP program,[41-43] using the PBE functional; a plane-wave basis set with an energy cut-off of 400 eV, PAW (Projector Augmented Wave)[44] treatment of core electrons and the VASP-supplied pseudopotentials for this method.[45] The same van der Waals correction as in the molecular calculations (D3BJ) was applied. Adsorption energies of the complex were compared by optimising the geometry of the complex on a slab consisting of three layers of Au, with a unit cell of 49 (7×7) atoms per layer. The uppermost Au layer was allowed to relax during these optimisations, while the lower two were frozen at the optimised bulk geometry. Dipole correction[46] was applied to the direction orthogonal to the surface.

RESULTS AND DISCUSSION

We have previously investigated the adsorption of (*S*)-proline on Au(111)[30] using low-temperature STM, HREELS and XPS. (*S*)-proline adsorbs weakly on Au(111) at 300 K. STM at 300 K is unable to image any molecular features owing to the high mobility of the adsorbed amino acid. At 77 K, the two-dimensional gas of proline condenses to form ordered arrangements of molecules which correspond to a mixture of the zwitterionic ($R\text{-}NH_2^+\text{-}COO^-$), neutral (non-zwitterionic) (R-NH-COOH) and anionic ($R\text{-}NH\text{-}COO^-$) proline forms. Desorption of proline occurs at relatively low temperature such that very few adsorbed species can be identified following annealing to 370 K.[30]

*STM*

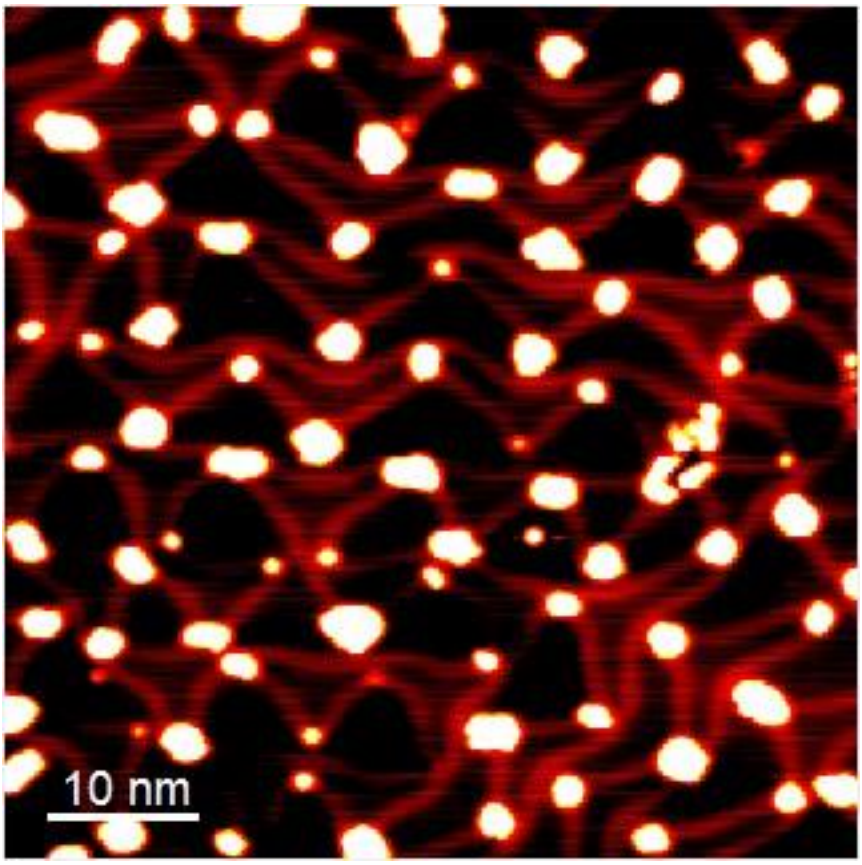


**Figure 2**. STM image acquired at 77 K showing the growth of Ni on Au(111) at 300 K. 56 nm × 56 nm, 0.99 V, 0.1 nA.

Figure 2 shows an STM image following the epitaxial growth of Ni on Au(111) at 300 K. 0.15 ML Ni was deposited at a rate of 0.005 ML $s^{-1}$ giving an average cluster size of 4.2 $nm^2$. Ni clusters are observed at the elbows of the herringbone reconstruction as first reported by Chambliss *et al*.[31] Subsequently, Meyer *et al*.[47] showed that the nucleation proceeds *via* a place exchange mechanism whereby a single gold atom is displaced by a diffusing Ni atom which acts as a nucleation point for island formation. Figure 3 shows a series of STM images (acquired after the sample was cooled to ~77 K) recorded as a function of annealing temperature following a 0.8 L dose of (*S*)-proline at 300 K onto 0.15 ML Ni/Au(111) (larger images are available in the

*Supporting Information*, Figure S1). Gao *et al*. reported that proline multilayers are not stable on the Pd(111) surfaces under these conditions.[8] Hence, we are able to conclude that a sub-monolayer proline coverage is present on the surface.

Figure 3A shows the surface after (*S*)-proline deposition. Significant etching of the 2-D Ni islands is apparent such that the number density of clusters decreases dramatically and only a few larger clusters remain. Molecular features are difficult to resolve and considerable streaking is observed which can be attributed to the rapid diffusion of molecular species. Similar behavior was reported following the adsorption of glutamic acid onto Ni/Au(111) by Trant *et al*.[18] After annealing to 340 K, circular molecular features are now resolvable with a diameter of ~6 Å (Figure 3B). There is no clear long range order though there is some evidence for the formation of disordered chains. After annealing to 370 K, similar molecular features are still observed and the Ni clusters are now so extensively etched that they are very difficult to identify (Figure 3C).

The STM image displayed in Figure 3D shows that annealing to 390 K yields evidence of the creation of ordered structures. Two distinct types of ordered arrangements are imaged. Firstly, chains possessing a width of two molecular features (~12 Å) and a typical length of up to 8 nm are observed. The second type of ordered phase imaged at this annealing temperature consists of a small number of 2D islands comprised of molecular features of ~6 Å in diameter. Annealing to 410 K (Figure 3E) results in a significantly more ordered surface that exhibits co-existing chains and 2D islands. The chains consist of molecular features exhibiting either a bright or a dark contrast. The brighter features are imaged as pairs of features with a nearest neighbor separation of ~7.5±1.0 Å. Adjacent pairs of bright features are separated by 20.0±1.0 Å.

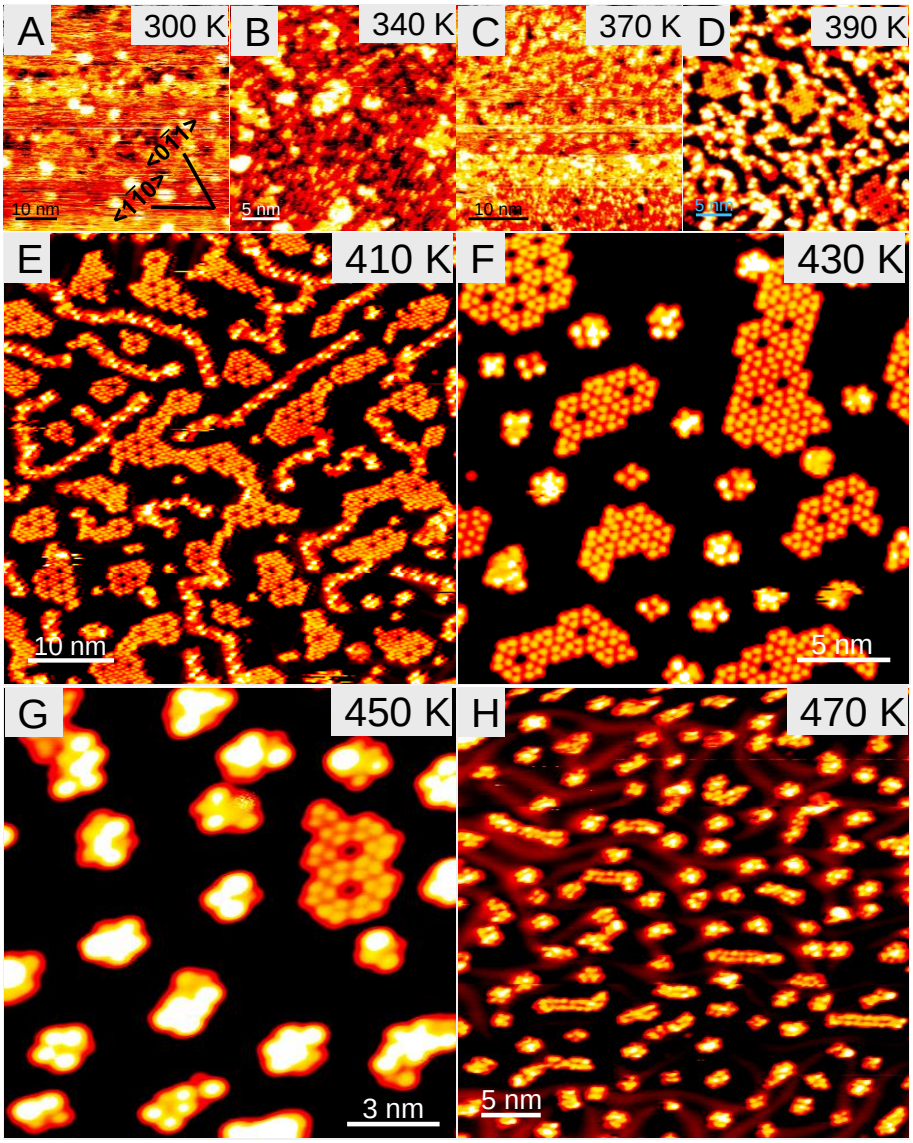


**Figure 3.** STM images acquired at 77 K after exposing (*S*)-proline to 0.15 ML Ni on Au(111) at 300 K as a function of annealing temperature. A) 300 K, 54.5 nm × 54.5nm, -0.67 V, 0.04 nA; B) 340 K, 29.4 nm × 29.4 nm, -0.61 V, 0.04 nA; C) 370 K, 53.3 nm × 53.3 nm, -0.67 V, 0.06 nA; D) 390 K, 31.3 nm × 31.3 nm, 0.67 V, 0.02 nA; E) 410 K, 52.3 nm × 52.3 nm, -0.70 V, 0.03 nA; F) 430 K, 24.3 nm × 24.3 nm, -0.63 V, 0.06 nA G) 450 K, 14.5 nm × 14.5 nm, 0.70 V, 0.03 nA; H) 470 K, 37.5 nm × 37.5 nm, -0.67 V, 0.11 nA

In the 2D islands, the molecular scale features image with a comparable contrast to the darker features observed in the chains. The pores observed in these islands are ~9 Å in diameter and are surrounded by six trimeric features in a hexagonal arrangement. We will henceforth refer to this structure as the hexagonal porous (HP) phase. The trimeric features possess approximately three-fold symmetry and, as will be discussed below, are the fundamental building blocks of the HP phase. Trimers most commonly abut three adjacent trimers to yield a porous molecular arrangement similar to that reported by Hooper *et al*. for 3-hydroxyphenalenone (3-HPLN) adsorption on Ag(111).[48]

After annealing to 410 K (Figure 3E), the surface coverage of molecular features drops significantly to ~45% from ~75% (390 K). Furthermore, there is a dramatic reduction in the number of molecular species accommodated in chains whilst there is a large increase in the area occupied by the HP phase. Following this annealing treatment there is a tendency for the pores within the HP phase to produce an ordered arrangement with a hexagonal unit cell which is consistent with a commensurate overlayer that can be described in matrix notation as <6 -1 | 1 5> *i.e.* with unit cell dimensions of 16.1 Å × 16.1 Å. The three rotationally equivalent domains of this structure are indistinguishable. It is noteworthy that no mirror domains are observed such that the islands of HP are locally chiral.

Figure 3F shows the surface after annealing to 430 K. Following this annealing treatment, the HP phase is the only ordered phase observed - no evidence is found for the presence of 1-D chains. Instead, there is an emergence of small bright clusters comprising less than ten molecular-scale features, all possessing a brighter contrast than the features making up the HP and chain phases. Further annealing to 450 K (Figure 3G) and 470 K (Figure 3H) results in a decrease in the coverage of HP phase and an increase in the relative abundance of the brighter

clusters, the total surface coverage falls from ~35 % to ~25%. In Figure 3G, the high resolution image of a small HP domain shows that each pore is surrounded by 6 units of three molecular features. Two adjacent pores share six of these molecular features. A feature consisting of three molecular units is imaged at the top left of the island. It is very important to note that such features are found to be the fundamental building block of each HP domain (See *Supporting Information*, Figure S2). The dimensions of the individual molecular components of the three-fold feature are consistent with that of a single proline molecule. We will show that the fundamental unit is a Ni(prolinate)$_3$ cluster. Annealing to 470 K results in the disappearance of all HP islands with only the bright clusters remaining that co-exist with a few chain-like entities that resemble the remnants of the HP phase.

*XPS*

Figure 4 shows the XP spectra obtained for the Ni $2p_{3/2}$; N 1s; C 1s and O 1s core levels following each annealing treatment. After deposition of 0.15 ML Ni onto Au(111), the Ni$2p_{3/2}$ core level (Figure 4A) exhibits a single peak at a binding energy (BE) of 852.1 eV which is in the range anticipated for metallic Ni.[49] Following exposure of (*S*)-proline at 300 K, there is a dramatic change in the Ni $2p_{3/2}$ line shape. The metallic Ni peak decreases in intensity and shifts to slightly higher BE (852.5 eV) and a new peak appears at 855.4 eV BE which corresponds to ~60% of the total Ni signal and is consistent with the presence of oxidized Ni species on the surface. The positions of the two features remain constant (to within ±0.1 eV) for each subsequent thermal treatment. The intensity of the 852.5 eV peak stays essentially constant with increasing annealing temperature and there is a significant decrease in the relative intensity of the higher BE feature from about 65% of the total Ni signal at 370 K to about 45% of the total signal at 450 K. The change in relative intensity can be assigned to the desorption of the Ni-containing

species that gives rise to the high BE peak. The loss of intensity of the oxidized Ni species could alternatively be explained by decomposition of the Ni containing species and diffusion of Ni into the bulk. We believe that this pathway is unlikely as the onset of Ni diffusion into the Au bulk was found to occur at >500 K.[50]

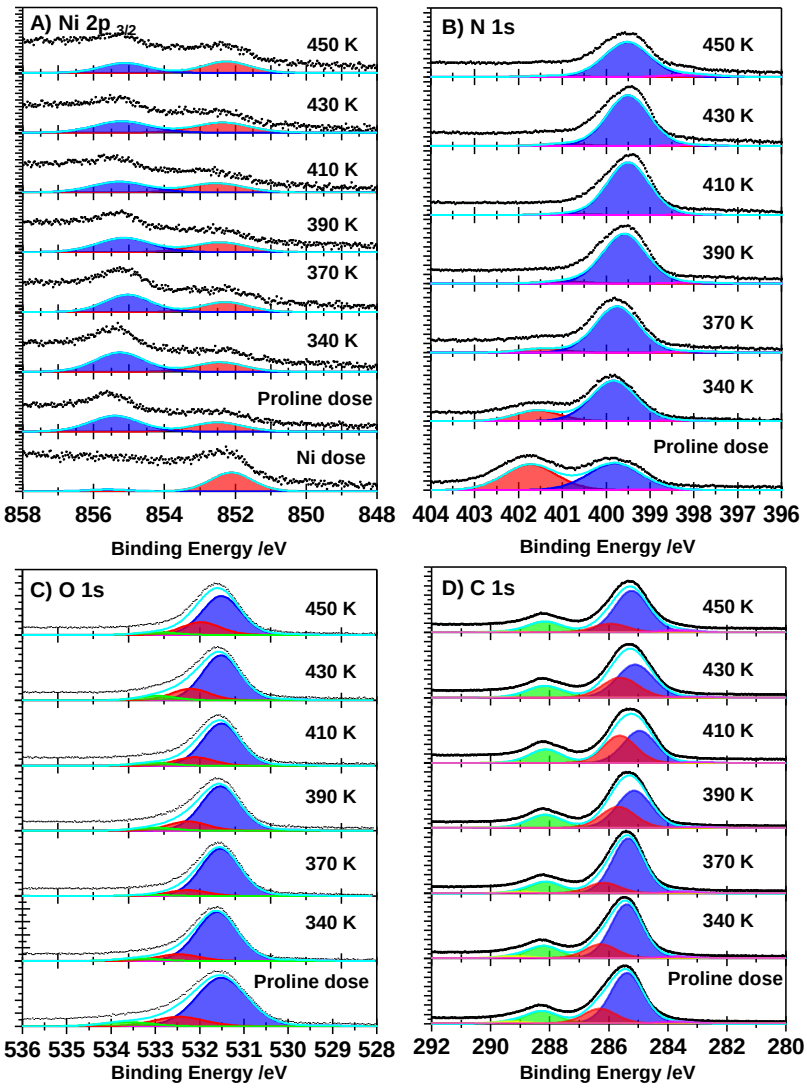


**Figure 4.** Ni $2p_{3/2}$ (A), N 1s (B), O 1s (C), and (D) C 1s XP spectra of (*S*)-proline on 0.15 ML Ni on Au(111) as a function of annealing temperature. For each spectrum the raw data are shown in black, the spectral components fitting the background subtracted data are shown as filled peaks, with the fitted envelope in cyan. Ni 2p region was also recorded prior to (*S*)-proline exposure.

Spectra were recorded normal to the surface at 300 K at different photon energies: A) 970 eV, B) 500 eV, C) 650 eV, and D) 400 eV.

The Ni core level BE is dependent on the ligating species, as is demonstrated in the work of Colpas *et al*.[51] whereby Ni(II) and Ni(III) complexes were compared with a range of different ligands. The paucity of literature for amino acid complexes of nickel makes it difficult to make a definitive assignment of oxidation state. We propose that the Ni is formally in the +3 oxidation state resulting in a charge-neutral complex. Although Ni(III) is not as common as the Ni(II) species, it is known that the Ni(III) can be stabilized by certain ligating species such as amines, carboxylates, sulfur-containing groups and peptides.[51] However, the BE of the Ni core level peak is also consistent with the presence of Ni(II) species.

Figure 4B shows the XP spectra for the N 1s core level. Following adsorption of (*S*)-proline, the spectrum consists of two peaks of similar intensity at 399.8 eV and 401.7 eV. Annealing to 340 K results in an increase in the relative intensity of the 399.8 eV BE feature. The 401.7 eV peak is barely detectable after annealing to 370 K and is not visible at higher annealing temperatures. With increasing annealing temperature, the 399.8 eV peak shifts down reaching 399.5 eV after annealing to 450 K at which temperature a significant decrease in peak intensity is also observed. In addition, after annealing to 450 K, a small shoulder appears at 398.2 eV BE. In similar studies of amino acids on metal surfaces, the higher BE feature has been assigned to the protonated $NH_2^+$ group of the zwitterionic form[29,52] and the lower BE feature is characteristic of the NH group more typical of the anionic species.[8,29] The disappearance of the zwitterionic feature in the N 1s spectrum after annealing to 390 K coincides with the onset of well-defined supramolecular assemblies in the STM images. We have shown that following the adsorption of proline onto Au(111),[30] essentially all molecular proline desorbs by 370 K. We therefore assign

the 401.7 eV feature to the presence of molecular proline in the zwitterionic form. Therefore, from the N 1s data, we are able to conclude that following annealing to 390 K and above, all proline contains an NH group hence is in either the anionic form or the neutral (non-zwitterionic) form.

The O 1s core level XP spectra are displayed in Figure 4C as a function of annealing temperature. At all annealing temperatures, a single asymmetric peak is present which was fitted with four components that were found to be present in the O 1s spectrum of proline on Au(111)[30]. The resulting spectra are comprised of four components analogous to the behavior of proline on Au(111)[30] and trimesic acid on Cu(111),[53] however, two of these features make up >90% of the total O 1s spectrum at each annealing temperature, whilst the two smaller components are barely visible but can be seen in the expanded spectra contained in the *Supporting Information (Figure S3)*. A large central feature at 531.5 eV BE contributes 70-90 % of the total oxygen signal at all stages of the experiment and can be assigned to the oxygen atoms of the electronically delocalized carboxylate species. Two significantly smaller features can be fitted at higher BE, one at 533.7 eV (hydroxyl oxygen; 7 %) and the second at 532.5 eV (carbonyl oxygen of the carboxylic acid moiety; 15 %). It should be noted that the hydroxyl oxygen could result from a low level of background water adsorption. The final peak forms a small shoulder to the large peak at 529.3 eV and never contributes more than 2% of the total oxygen signal. The BE of the main component of the O 1s signal was found to remain essentially constant (within ±0.1 eV) throughout the annealing treatments. From the spectral components of the O 1s core level, we can conclude that the majority of adsorbed proline contains the carboxylate functionality with a delocalized electronic charge while some exists with the carbonyl group intact either as part of a O=C-OH or a O=C-$O^-$ functionality. Since the high BE

feature attributed to the hydroxyl group never contributes more than ~7% of the total oxygen signal and after annealing to 390 K all the nitrogen exists as NH, it is clear that almost all proline species are present in the anionic form, mainly existing in the delocalized carboxylate form with a small contribution from prolinate species containing the O=C-O$^-$ functionality. There are negligible levels of neutral or zwitterionic proline present. This is consistent with the behavior of proline on Au(111) in the absence of Ni[30] where molecular desorption/decomposition occurred at 370 K. Thus we infer that all proline present on the surface above this temperature in this study is adsorbed to residual Ni clusters or bound to a Ni ion in an organometallic complex.

Figure 4D shows the C 1s XP spectra as a function of annealing temperature. Two relatively broad peaks are resolvable in the unfitted spectra. As with the O and N 1s spectra, the C 1s spectra are broadly similar to those we reported for proline on Au(111).[30] On Au, five peaks were resolved at binding energies of 283.2 eV (a low intensity feature); 285.1 and 286.0 eV (two peaks of similar (relatively high) intensity); 287.9 eV and 289.3 eV.[39] On Ni/Au(111), the C 1s spectra are less well resolved, with only two asymmetric peaks being visible in the unfitted spectra. Each of these peaks contain contributions from two components by analogy with the study on Au(111).[30] The larger peak contains contributions from components of similar intensity at 286.1 and 285.3 eV (corresponding to carbon atoms of the pyrrolidine ring), with a small low BE peak at 284.0 eV. After annealing to 390 K, the component at 286.1 eV becoming relatively more intense whilst the component at 285.3 eV becomes less intense. The integrated intensity of these two peaks remains constant (~40 % of the total C 1s signal). The presence of multiple prolinate species on the surface and residual Ni clusters make drawing conclusions on ring-orientation from relative intensities extremely difficult.

The smaller component at a BE of 288.3 eV was fitted with two components (in line with the study of proline on Au(111)[30]) and can be assigned to the carboxylate functionality (288.3 eV) with a small, almost negligible, contribution from the carboxylic acid functionality (289.7 eV).[30] The intensity and BE of the 288.3 eV peak stays essentially constant with increasing annealing temperature.

From XPS, we may conclude that, after annealing to 390 K to remove unreacted zwitterionic proline, the surface is covered in nickel prolinate complexes. The presence of the trimeric features in the STM images suggests the possibility that Ni(prolinate)$_3$ species have been formed. If such species contain Ni(III) ions, the overall charge would be neutral. If the oxidation state of Ni is +2, the species would have an overall negative charge.

Trimeric features of this type of structure were never observed following proline adsorption on Au(111),[30] hence the molecular array is stabilized by the presence of Ni. Most commonly, amino acids deprotonate on single crystal metal surfaces and adsorb in the anionic form[10,54,55] and the annealing temperature required to form the HP phase is significantly above the desorption temperature of $H_2$ from either Ni or Au surfaces. Hence, it is likely that the proline species present in the HP phase are in the anionic form. In order to achieve a charge balance the most logical explanation is that the trimers correspond to a Ni(prolinate)$_3$ complex with the Ni ion bearing a formal positive charge.

*DFT*

It is known that proline can form stable octahedral anionic complexes with Ni and a stabilizing countercation[56] with a similar structure to that of Co(prolinate)$_3$.[57] In each of these complexes, each proline ligand is coordinated to the central metal ion *via* the lone pair of electrons on the NH species and an O atom of the O-C=O functionality. The six chelating atoms adopt an

octahedral environment around the central ion.[56-58] It should be noted that Kong *et al* [59] describe topologically similar Ni-containing bioinorganic complexes on Au(111). The authors attribute, through STM and DFT calculations, these structures to a hydrogen-bonded cytosine trimer around a $Ni_3$ core with each Ni atom having an oxidation state of zero. A similar complex was considered for the Ni-prolinate complex, however, the spectroscopic evidence, particularly the Ni 2p XP spectra, does not support this theory. Unlike the cytosine trimers, which are only imaged as isolated structures, the Ni-prolinate complexes prefer to pack together forming 1-D or 2-D networks.

An octahedral $Ni(prolinate)_3$ complex analogous to $Co(prolinate)_3$[58] would be of the type $M(AB)_3$ where A and B are chelating atoms from within the same molecule. Complexes with this structure can exist as two possible stereoisomers, of which two are pairs of enantiomers as illustrated in Figure 5.

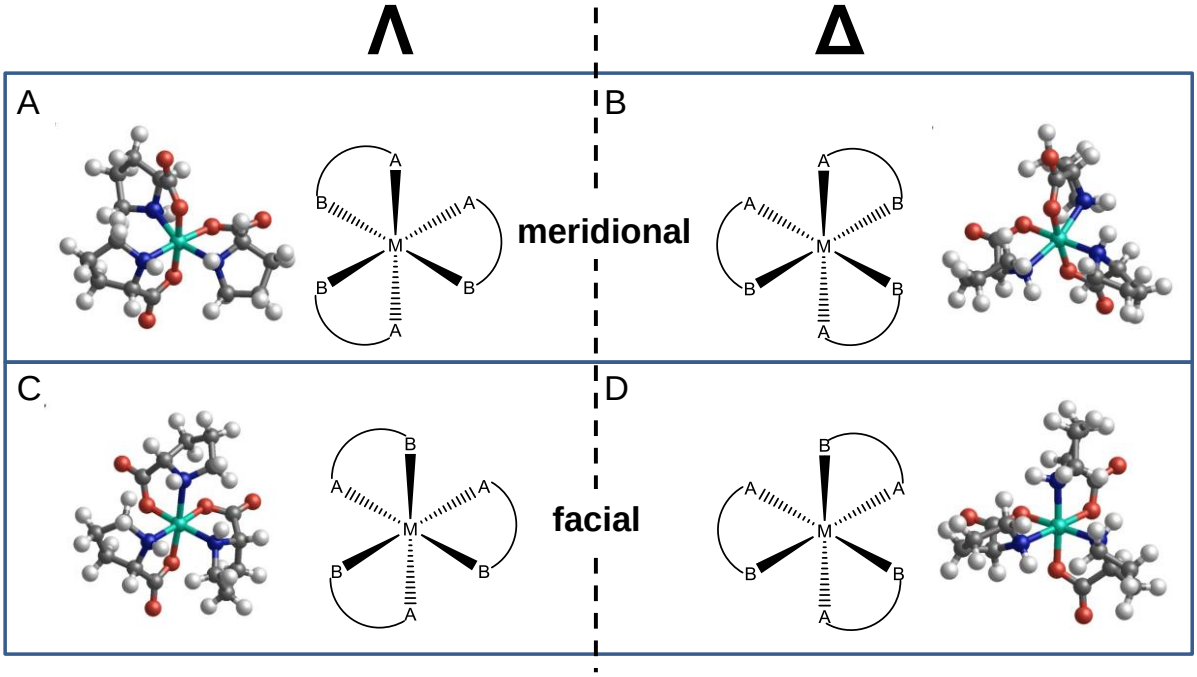

**Figure 5**. Schematic representation of all possible isomers of an octahedral complex with three identical bidentate ligands ($M(AB)_3$)with the corresponding optimised 3-D models of Ni(prolinate)$_3$. A – Λ-*mer*, B – Δ-*mer*, C – Λ-*fac*, and D – Δ-*fac*.

If all three chelating N atoms are above a plane going through the center of the Ni ion and all three chelating O atoms are below this plane, the facial (*fac*) isomer of Ni(prolinate)$_3$ is defined (Figure 5). The other possible arrangement of N and O atoms gives the meridional (*mer*) isomer whereby three N atoms are contained in the equatorial plane (Figure 5). A complicating factor when describing the 3-D structures of these complexes is that although, for example, the Δ-*fac*- and Λ-*fac*-isomers are mirror images in terms of the chelating atoms, the chirality of the proline ligands removes the mirror relationship between the two isomers. Furthermore, in the gas phase, an isolated proline molecule can exist as either *cis*- or *trans*-isomers; in the *trans*-isomer the carboxylic acid moiety is in the same plane as the pyrrolidine ring, whereas in the *trans*-isomer they are in different planes. The DFT calculations only considered the *cis*-conformer bound to the Ni ion since this is the conformer found in the crystal structures of proline[60] and Co(prolinate)$_3$.[57]

From the point of view of their interaction with the Au surface, the key difference between the isomers is the relative position of the three pyrrolidine rings to each other, this will affect not only the stability of the complex but also the adsorption footprint, along with interactions between neighboring complexes.

DFT calculations were carried out to ascertain the relative stability of all four-isomers in the gas phase and also of each isomer adsorbed onto an Au slab (Table 1) and Figure 6. Calculations were carried out on isolated adsorbed species and do not take into account interactions between adjacent Ni(prolinate)$_3$ units.

In the gas phase, the *mer* isomers were found to be most stable, with very little difference in energy between Λ and Δ. The Δ-*fac*-enantiomer is more stable than the Λ-*fac*-enantiomer by ~25 kJ mol$^{-1}$. The likely bonding configuration of these species with the Au surface would be *via* the carboxylate functionalities. Surprisingly, we found that the relative energies of both the two facial and the two meridional enantiomers are reversed on adsorption. We anticipated that there would be very little difference in adsorption energy as the relative position of the pyrrolidine rings has negligible impact on the interaction of the molecule with the surface.

**Table 1.** Comparison of Energies Calculated by DFT of the Stereoisomers of Ni(prolinate)$_3$ in the Gas Phase and on a Gold Slab, in kJ mol$^{-1}$

| | Gas phase | Surface |
|---|---|---|
| Δ-*fac* | 23.2 | 37.8 |
| Λ-*fac* | 47.8 | 16.8 |
| Δ-*mer* | 0.0 | 62.6 |
| Λ-*mer* | 2.2 | 0.0 |

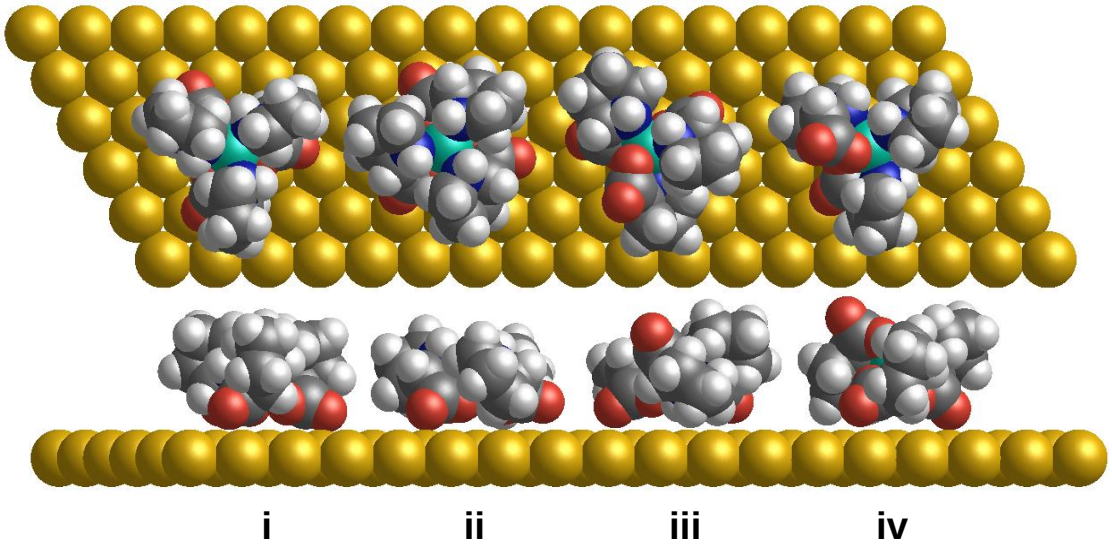

**Figure 6.** Views from above and side-on of 3-D models of each possible stereoisomers of the Ni(prolinate)$_3$ trimers optimised in the gas phase and superimposed onto an Au slab. i - Δ-*fac*, ii - Λ -*fac* , iii - Λ -*mer*, iv - Δ -*mer*

However, the calculations reveal that the adsorbed Λ-*fac*- enantiomer is more stable than the Δ-*fac*- enantiomer by 21 kJmol$^{-1}$. We therefore conclude that the Λ-*fac* isomer is thermodynamically favored over the Δ-*fac*- enantiomer when adsorbed on the Au surface. The three fold symmetry of the facial isomers is similar to that observed in the HP phase, so we conclude that the HP phase is constructed from Λ-*fac* -isomers. On a relatively unreactive surface such as Au, intermolecular interactions are often critical in determining the relative thermodynamic stability of different ordered arrangements. If intermolecular interactions are taken into account, it is likely that the relative abundance of adsorbed Λ-*fac* –isomers over the Λ–*mer* isomers can be explained despite the fact that the latter has a more favourable adsorption energy as an isolated species.

It is clear from the STM images that the trimers can stack in various different ways, some of them producing hexagonal pores characteristic of the HP phase. It is also possible to stack the trimers in denser arrangements forming 'pore-less' islands. As Figure S2 shows (*Supporting Information*), trimers are able to assemble into 1-D chains but these are morphologically distinct from the 1-D chains shown in Figure 3E . The Δ-*mer* species, which is the most stable in the gas phase, is found to be the least stable species on the surface, so we do not expect this to be present to any significant extent in the observed phases. The meridional isomers can be described as having two of the three carboxylates on one side of the Ni ion and the third on the opposite side. If the interaction with the surface is dominated by the carboxylate moieties, it seems likely that

the optimum adsorption geometry would involve two carboxylates binding to the surface with the third pointing away from the surface.

In the STM image of the chains of molecular features, an alternation of features exhibiting bright and dark contrast is observed with two darker features being observed for every bright feature. We conclude that the chains are constructed from meridional (Λ -*mer*) isomers and that the bright features are associated with the carboxylate groups pointing away from the surface .

*HREELS*

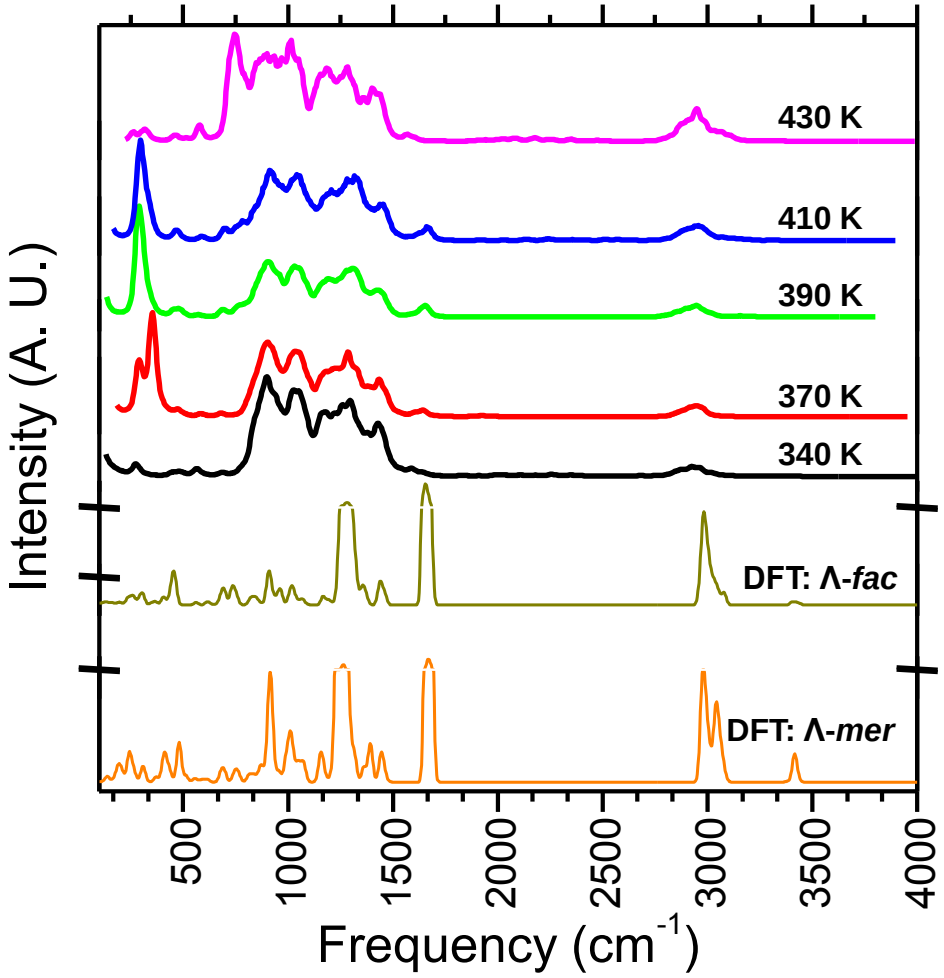


**Figure 7.** Enhanced HREEL spectra of (*S*)-proline exposed at 300 K to approximately 0.2 ML Ni on Au(111) as a function of annealing temperature. All spectra were recorded at 300 K. The lower two spectra are theoretical vibrational spectra of isomers of Ni(prolinate)$_3$. In these cases, the more intense features have been truncated to allow the weaker features to be observed.

The HREEL spectra in Figure 7 were acquired at 300 K after exposing ~0.2 ML Ni on Au(111) to (*S*)-proline at 300 K and as a function of annealing temperature. After deposition and annealing to 340 K, loss features are observed at 276, 901, 1026, 1181, 1226, 1261, 1296, 1431,

1591 and 2926 $cm^{-1}$. After annealing to 370 K, the 276 $cm^{-1}$ peak increases in intensity and an intense low frequency peak is observed at 355 $cm^{-1}$. In addition, a small peak is observed at 1635 $cm^{-1}$ replacing the peak at 1591 $cm^{-1}$.

Annealing to 390 K and 410 K results in a shift in the position of this peak to 1655 $cm^{-1}$ and a decrease in the intensity of the 355 $cm^{-1}$ peak. Annealing to 430 K results in the almost complete disappearance of the 276, 355 and 1655 $cm^{-1}$ features and the appearance of a new peak at 745 $cm^{-1}$.

**Table 2**. Summary and Assignment of Peaks Observed in HREELS Experiment of (*S*)-Proline on 0.15 ML Ni on Au(111) as a Function of Annealing Treatment

| Proline Au(111) | Proline On Ni/Au(111) | | | | | DFT | | |
|---|---|---|---|---|---|---|---|---|
| 300 K | 340 K | 370 K | 390 K | 410 K | 430 K | Λ-fac | Λ-mer | Assignments |
| 3710 | | | | | | 3401 | 3417 | ν(N-H) |
| | 2926 | 2945 | 2950 | 2956 | 2950 | 2982 | 2978 | $\nu_{as}(CH_2)$ |
| | | 1645 | 1655 | 1661 | | 1678 | 1671 | ν(C1=O2) |
| 1620 | 1591 | | | | 1570 | | | |
| 1390 | 1431 | 1435 | 1425 | 1436 | 1400 | | | |
| | | | 1310 | 1316 | | 1320 | | $\nu(C^4\text{-}C^5)$, $\omega(C^5H_2)$, |
| | 1296 | 1285 | | 1281 | 1285 | | 1299 | $\upsilon(C^1\text{-}C^2)$, ω(CH), $\tau CH_2$), ω(N-H), $\tau(C^5H_2)$, |
| | 1181 | | 1195 | 1206 | 1185 | | 1194 | $\tau(C^3H_2)$, $\tau(C^5H_2)$, $\omega(C^2H)$, ω(N-H) |
| | 1026 | 1035 | 1030 | 1041 | 1015 | 1019 | | Pyr as breath (ring deformations) |
| | | | | | 970 | 962 | | Pyr as breath (ring deformations) |
| | | | | | 935 | | 921 | $\upsilon(C^1\text{-}C^2)$, pyr as breath |
| | 901 | 900 | 900 | 911 | 900 | 899 | | Pyr as breath (ring deformations) |
| | | | | 781 | 745 | 752 | | $\nu(Ni\text{-}O^1)$, $\delta_{sciss}(O^2\text{-}C^1\text{-}O^1)$, $\omega(C^1)$ |
| | | | 690 | 696 | | 691 | | Chel deformation ($\nu(Ni\text{-}O^1)$ δ(C1)) |
| | 686 | 680 | | | | | 687 | pyr deformations |
| | | 585 | | 581 | 580 | | 588 | $\rho(C^4H_2)$ |
| | 566 | | 570 | | | 561 | | $\nu_{as}(O^1\text{-Ni-N})$ |
| | 481 | 470 | 480 | 461 | 460 | | 435 | Pyr buckle, breath and deform of chel |
| | | 355 | | | | 348 | | As breath of chel |
| | | 290 | 290 | 296 | 315 | 306 | | $\nu_{as}(N\text{-Ni-}O^1)$ |
| | 276 | | | | 265 | 260 | | $\nu(Ni\text{-}O^1)$, pyr buckle |

ρ = rock, ν = stetch, ω = wag, δ = bend, τ = twist, as = asymmetric, s = symmetric, breath = ring breathing, pyr = pyrrolidine ring, chel = chelating ring.

Table 2 shows the assignments of the vibrational bands. In addition, calculated vibrational spectra for the gas phase Λ-*mer* and Λ-*fac* Ni(prolinate)$_3$ complexes are shown in Figure 7 and the vibrational frequencies are displayed in Table 2. A comprehensive list of vibrations and assignments are available in Table S1 (*Supporting Information*). There is good agreement between the bands predicted from the DFT calculation and the loss features observed in the HREEL spectra. The DFT simulation predicts bands at 260 and 306 associated with the Ni-O stretching mode) and a carbonyl band at 1678 or 1671 cm$^{-1}$. The loss features in the HREEL spectra at ~1650 cm$^{-1}$ are significantly higher in frequency than is typical for an asymmetric carboxylate stretching frequency.[54] In the DFT calculations, a band at this frequency is one of the most intense and is assigned to the C=O stretch of the carbonyl groups. In the experimental HREEL spectra, though present, this band is relatively weak.

The most likely explanation is that this band corresponds to the carbonyl group of the *mer* trimer which is not involved in bonding with the surface. In the experimental data a relatively intense band is observed in the 1420-1440 cm$^{-1}$ range. In the DFT calculation, no intense feature is predicted at this frequency.

This band can be assigned to the symmetric stretching mode of the carboxylate moiety[11] and may contain a contribution from the presence of prolinate species on residual nickel clusters. However, the weak carbonyl feature in the HREEL spectra coupled with the intense carboxylate feature in the XPS spectra suggest that the Ni(prolinate)$_3$ species are bonded to the surface *via* delocalized carboxylate functionalities rather than O-C=O functionalities as exist in the gas phase prolinate complexes. The combination of experimental data and computational analysis enable us to propose the following mechanism for the formation of the HP phase and the 1-D chains. Proline adsorbs onto the Ni clusters and removes Ni atoms from the edges of the clusters.

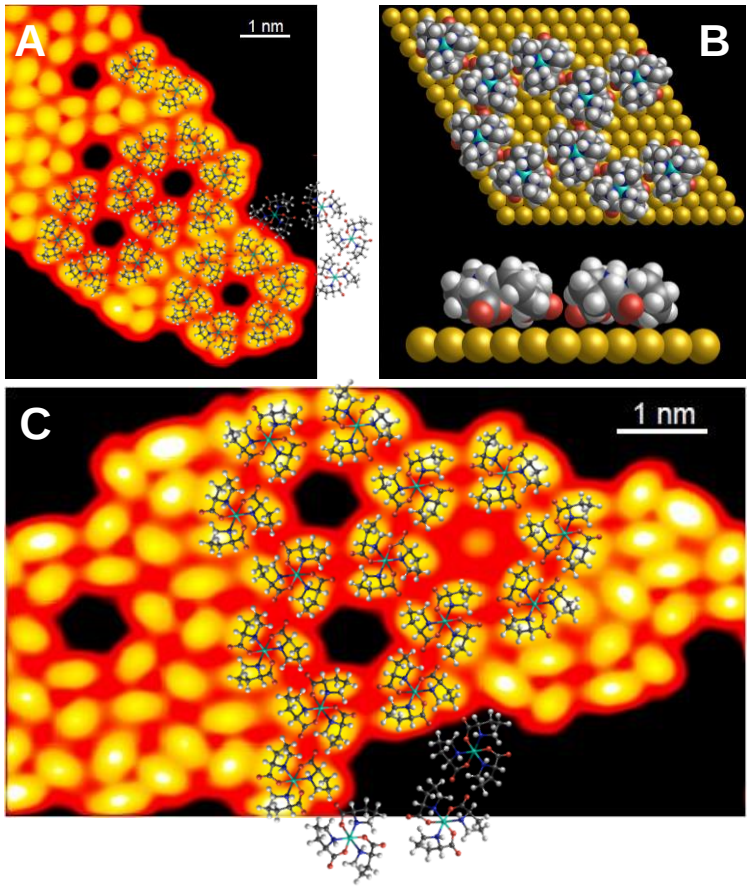


**Figure 8.** (A) Overlay of the trimer features onto the STM image (0.-63 V, 0.06 nA) of a domain of the HP phase. (B) Proposed unit cell of the HP phase from viewed from above and side-on. (C) Overlay of Λ-*fac* trimers on an STM image (0.73 V, 0.04 nA) showing regular elongation of prolinate features.

Proline is deprotonated and oxidizes Ni to either Ni(II) or Ni(III) leading to the formation of Ni(prolinate)$_3$ complexes which are either charge neutral or possess a nominal single negative charge – *i.e.* analogous to prolinate adsorption on Cu(110)[10] and Au(111).[30] Two types of adsorbed bioinorganic complexes are favored - When adsorbed onto the Au(111) surface, the Λ-*fac* - and Λ-*mer* isomers are favored over the Δ forms. Initially, these are present as a random mixture on the surface. Upon annealing, the two types of cluster segregate into separate regions

forming the 2-D HP phase (bound to the surface by three carboxylate groups, Figure 8) and the 1-D chains (bound to the surface via two carboxylate groups with the third pointing away from the surface, Figure 9).

At the highest annealing temperature (450 K); the HP phase disappears and the only residual features on the surface are bright nano-sized clusters made up of individual molecular features. There is a decrease in the intensity of the higher BE feature in the Ni $2p_{3/2}$ XP spectra and a decrease also in the intensity of the C, N and O core level peaks. The identification of the chemical composition of these clusters requires further work – it is likely that they are the result of surface decomposition and/or polymerization.

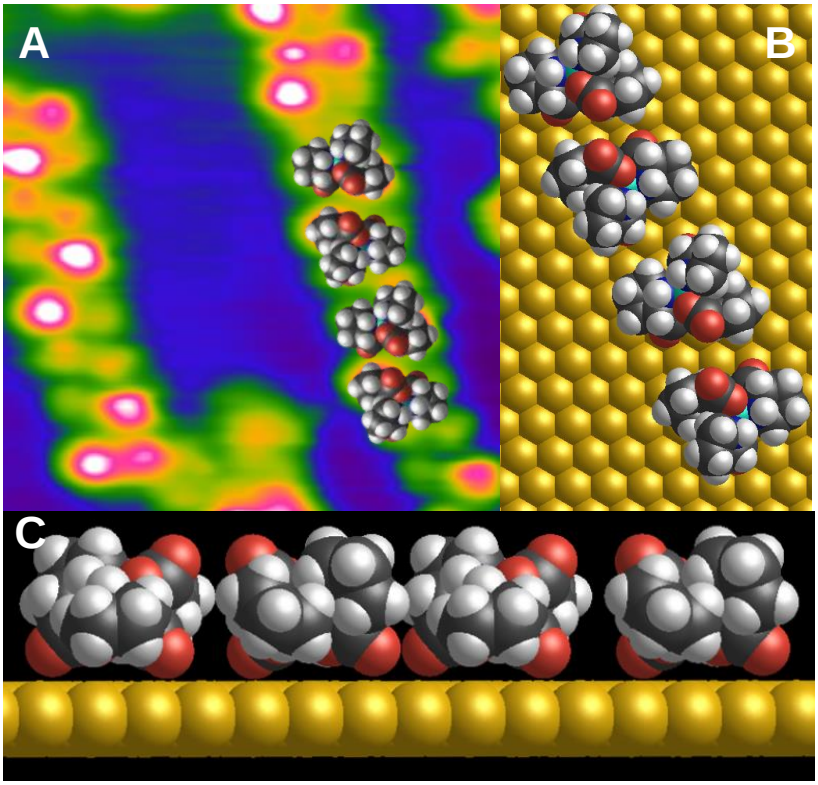


**Figure 9.** (A) Overlay of Λ-*mer* trimers on an STM image (-0.61 V, 0.06 nA) of 1-D chains to highlight the periodic variation in contrast, (B) Λ-*mer* isomer of proline arranged on a Au slab to

match dimensions and features of (A) and (C) side-on view of chain showing the proline with the upright carboxylate causing the brighter contrast.

## CONCLUSIONS

The adsorption of (*S*)-proline onto 2-D Ni clusters nucleated at the elbows of the Au(111) herringbone reconstruction results in the corrosion and oxidation of Ni. At room temperature, proline exists as a mixture of zwitterionic, anionic and neutral species. Annealing to 390 K results in a transformation of the zwitterionic component into the anionic form. STM reveals that annealing also results in the formation of two distinct types of ordered structure. One phase is characterized by hexagonal pores (HP phase). The second ordered phase is composed of 1-D chains of pairs of features alternating in contrast. The fundamental building block of these phases corresponds to trimeric features which we conclude are Ni(prolinate)$_3$ complexes. The difference in morphology of the phases is attributed to each phase being composed of different isomeric forms of the trimers.

The HP phase is constructed from Λ-*fac*-tris((*S*)-prolinato)nickel(III) which has $C_3$ symmetry whilst the chains are constructed from arrangement of Λ-*mer*-tris((*S*)-prolinato)nickel(III), which has one carbonyl elevated with respect to the rest of the complex causing the difference in contrast.

At high temperature, clusters comprising a few molecular features are formed; possibly *via* a surface mediated polymerization process. It is unclear whether these nanoclusters are preferentially formed by one isomer or the other however the appearance of the nanoclusters corresponds to the loss of chains. Since the Ni clusters do not reappear, it is likely that the trimers desorb intact and therefore that the less strongly bound Λ-*fac* isomers will desorb preferentially.

ASSOCIATED CONTENT

**Supporting Information**. Expanded XP spectra and STM images, further STM trimer evidence and full table of vibrational assignments. This material is available free of charge *via* the Internet at http://pubs.acs.org.

AUTHOR INFORMATION


### Corresponding Author

* Email: cjb14@st-andrews.ac.uk

### Present Addresses

§ Celestijnenlaan 200F, B-3001 Heverlee, Belgium.


### Author Contributions

The manuscript was written through contributions of all authors. All authors have given approval to the final version of the manuscript. /

ACKNOWLEDGMENT


RTSG and JG acknowledge the Engineering and Physical Sciences Research Council (EPSRC, UK) for the award of a PhD studentship. The research leading to these results has received funding from the European Community's Seventh Framework Programme (FP7/2007-2013) under grant agreement nş 312284. We thank EaStCHEM for computational support *via* the EaStCHEM Research Computing Facility


REFERENCES

1. Lam, H.; Oh, D.-C.; Cava, F.; Takacs, C. N.; Clardy, J.; de Pedro, M. A.; Waldor, M. K. D-Amino Acids Govern Stationary Phase Cell Wall Remodeling in Bacteria. *Science* **2009**, 325, 1552-1555.

2. Siegel, J. S. Homochiral Imperative of Molecular Evolution. *Chirality (New York, N.Y.)* **1998**, 10, 24-27.

3. Avalos, M.; Babiano, R.; Cintas, P.; Jimenez, J. L.; Palacios, J. C. Symmetry Breaking by Spontaneous Crystallization--is it the Most Plausible Source of Terrestrial Handedness We Have Long Been Looking For?--A Reappraisal. *Origins Life Evol. Biosphere* **2004**, 34, 391-405.

4. Weissbuch, I.; Bolbach, G.; Leiserowitz, L.; Lahav, M. Chiral amplification of oligopeptides *via* polymerization in two-dimensional crystallites on water. *Origins Life Evol. Biosphere* **2004**, 34, 79-92.

5. Rosi, N. L.; Mirkin, C. A. Nanostructures in Biodiagnostics. *Chem Rev* **2005**, 105, 1547-1562.

6. Izumi, Y. Modified Raney-Nickel (MRNi) Catalyst - Heterogeneous Enantio-Differentiating (Asymmetric) Catalyst. *Adv Catal* **1983**, 32, 215-271.

7. Eralp, T.; Shavorskiy, A.; Zheleva, Z. V.; Held, G.; Kalashnyk, N.; Ning, Y.; Linderoth, T. R. Global and Local Expression of Chirality in Serine on the Cu{110} Surface. *Langmuir* **2010**, 26, 18841-18851.

8. Gao, F.; Wang, Y. L.; Burkholder, L.; Tysoe, W. T. Chemistry of L-Proline on Pd(111): Temperature-Programmed Desorption and X-ray Photoelectron Spectroscopic Study. *Surf. Sci.* **2007**, 601, 3579-3588.

9. Forster, M.; Dyer, M. S.; Persson, M.; Raval, R. Probing Conformers and Adsorption Footprints at the Single-Molecule Level in a Highly Organized Amino Acid Assembly of (S)-Proline on Cu(110). *J. Am. Chem. Soc.* **2009**, 131, 10173-10181.

10. Marti, E. M.; Barlow, S. M.; Haq, S.; Raval, R. Bonding and Assembly of the Chiral Amino Acid S-Proline on Cu(110): The Influence of Structural Rigidity. *Surf. Sci.* **2002**, 501, 191-202.

11. Haq, S.; Massey, A.; Moslemzadeh, N.; Robin, A.; Barlow, S. M.; Raval, R. Racemic versus enantiopure alanine on Cu(110): An Experimental Study. *Langmuir* **2007**, 23, 10694-10700.

12. Jones, G.; Jones, L. B.; Thibault-Starzyk, F.; Seddon, E. A.; Raval, R.; Jenkins, S. J.; Held, G. The Local Adsorption Geometry and Electronic Structure of Alanine on Cu{110}. *Surf. Sci.* **2006**, 600, 1924-1935.

13. Barlow, S. M.; Louafi, S.; Le Roux, D.; Williams, J.; Muryn, C.; Haq, S.; Raval, R. Polymorphism in Supramolecular Chiral Structures of R- and S-alanine on Cu(110). *Surf. Sci.* **2005**, 590, 243-263.

14. Kuhnle, A.; Linderoth, T. R.; Hammer, B.; Besenbacher, F. Chiral Recognition in Dimerization of Adsorbed Cysteine Observed by Scanning Tunnelling Microscopy. *Nature* **2002**, 415, 891-893.

15. Eralp, T.; Shavorskiy, A.; Held, G. The Adsorption Geometry and Chemical State of Lysine on Cu{110}. *Surf. Sci.* **2011**, 605, 468-472.

16. Eralp, T.; Shavorskiy, A.; Zheleva, Z. V.; Dhanak, V. R.; Held, G. Hydrogen Bond-Induced Pair Formation of Glycine on the Chiral Cu{531} Surface. *Langmuir* **2010**, 26, 10918-10923.

17. Thomsen, L.; Wharmby, M. T.; Riley, D. P.; Held, G.; Gladys, M. J. The Adsorption and Stability of Sulfur Containing Amino Acids on Cu{531}. *Surf. Sci.* **2009**, 603, 1253-1261.

18. Trant, A. G.; Jones, T. E.; Baddeley, C. J. Thermal Treatment of Glutamic Acid-Modified Nickel Nanoclusters on Au{111} Leads to the Formation of One-Dimensional Metal-Organic Coordination Networks. *J. Phys. Chem. C* **2007**, 111, 10534-10540.

19. Jones, T. E.; Baddeley, C. J.; Gerbi, A.; Savio, L.; Rocca, M.; Vattuone, L. Molecular Ordering and Adsorbate Induced Faceting in the Ag{110}-(S)-Glutamic Acid System. *Langmuir* **2005**, 21, 9468-9475.

20. Jones, T. E.; Urquhart, M. E.; Baddeley, C. J. An Investigation of the Influence of Temperature on the Adsorption of the Chiral Modifier, (S)-Glutamic acid, on Ni{111}. *Surf. Sci.* **2005**, 587, 69-77.

21. Zhao, X. Y. Fabricating Homochiral Facets on Cu(001) with L-lysine. *J. Am. Chem. Soc.* **2000**, 122, 12584-12585.

22. Wilson, K. E.; Früchtl, H. A.; Grillo, F.; Baddeley, C. J. (S)-Lysine Adsorption Induces the Formation of Gold Nanofingers on Au{111}. *Chem Commun* **2011**, 47.

23. Wilson, K.; Baddeley, C. Chiral Assemblies of Nickel Lysinate *via* the Corrosive Adsorption of (S)-lysine on Ni/Au {111}. *Surf. Sci.* **2014**, 629, 102-107.

24. Remko, M.; Fitz, D.; Broer, R.; Rode, B. M. Effect of Metal Ions (Ni(2)(+), Cu(2)(+) and Zn(2)(+)) and Water Coordination on the Structure of L-Phenylalanine, L-Tyrosine, L-Tryptophan and Their Zwitterionic Forms. *J Mol Model* **2011**, 17, 3117-28.

25. Trant, A. G.; Baddeley, C. J. Chiral Recognition at One-Dimensional Metal-Organic Coordination Networks Initiates the Ordering of Prochiral Catalytic Reagent Methylacetoacetate on Au{111}. *Langmuir* **2011**, 27, 1788-1795.

26. Besson, M.; Pinel, C. Diastereoselective Catalytic Hydrogenation on Heterogeneous Metal Catalysts. *Topics in Catalysis* **1998**, 5, 25-38.

27. Exl, C.; Ferstl, E.; Honig, H.; RogiKohlenprath, R. Diastereoselective Hydrogenations of Unsymmetrically Substituted Aromatics. *Chirality* **1995**, 7, 211-218.

28. Fleming, G. J.; Adib, K.; Rodriguez, J. A.; Barteau, M. A.; White, J. M.; Idriss, H. The Adsorption and Reactions of the Amino Acid Proline on Rutile $TiO_2$(010) Surfaces. *Surf. Sci.* **2008**, 602, 2029-2038.

29. Fleming, G. J.; Adib, K.; Rodriguez, J. A.; Barteau, M. A.; Idriss, H. Proline Adsorption on $TiO_2$(110) Single Crystal Surface: A Study by High Resolution Photoelectron Spectroscopy. *Surf. Sci.* **2007**, 601, 5726-5731.

30. Seljamäe-Green, R. T.; Simpson, G. J.; Grillo, F.; Greenwood, J.; Francis, S. M.; Schaub, R.; Lacovig, P.; Baddeley, C. J. Assembly of a Chiral Amino Acid on an Unreactive Surface: (S)-Proline on Au(111). *Langmuir* **2014**, 30, 3495-3501.

31. Chambliss, D.; Wilson, R.; Chiang, S. Nucleation of ordered Ni island arrays on Au(111) by surface-lattice dislocations. *Phys. Rev. Lett.* **1991**, 66, 1721-1724.

32. Frederick, B. G.; Jones, T. S.; Pudney, P. D. A.; Richardson, N. V. Hreels and Rairs - a Complete Vibrational Study of the Surface Benzoate Species Adsorbed on Copper. *J. Electron. Spectrosc. Relat. Phenom.* **1993**, 64-5, 115-122.

33. Frederick, B. G.; Richardson, N. V. Ultrahigh-Resolution Electron-Energy-Loss Spectroscopy - Comment. *Phys. Rev. Lett.* **1994**, 73, 772-772.

34. Baraldi, A.; Barnaba, M.; Brena, B.; Cocco, D.; Comelli, G.; Lizzit, S.; Paolucci, G.; Rosei, R. Time Resolved Core Level Photoemission Experiments with Synchrotron Radiation. *J. Electron. Spectrosc. Relat. Phenom.* **1995**, 76, 145-149.

35. Baraldi, A.; Comelli, G.; Lizzit, S.; Kiskinova, M.; Paolucci, G. Real-Time X-ray Photoelectron Spectroscopy of Surface Reactions. *Surf. Sci. Rep.* **2003**, 49, 169-224.

36. Cautero, G.; Sergo, R.; Stebel, L.; Lacovig, P.; Pittana, P.; Predonzani, M.; Carrato, S. A Two-Dimensional Detector for Pump-and-Probe and Time Resolved Experiments. *Nucl Instrum Meth A* **2008**, 595, 447-459.

37. Barth, J. V.; Brune, H.; Ertl, G.; Behm, R. J. Scanning Tunneling Microscopy Observations on the Reconstructed Au(111) Surface - Atomic-Structure, Long-Range Superstructure, Rotational Domains, and Surface-Defects. *Phys. Rev. B* **1990**, 42, 9307-9318.

38. Perdew, J. P.; Burke, K.; Ernzerhof, M. Generalized Gradient Approximation made Simple. *Phys. Rev. Lett.* **1996**, 77, 3865-3868.

39. Grimme, S.; Ehrlich, S.; Goerigk, L. Effect of the Damping Function in Dispersion Corrected Density Functional Theory. *J. Comput. Chem.* **2011**, 32, 1456-65.

40. Weigend, F.; Ahlrichs, R. Balanced Basis Sets of Split Valence, Triple Zeta Valence and Quadruple Zeta Valence Quality for H to Rn: Design and Assessment of Accuracy. *Phys. Chem. Chem. Phys.* **2005**, 7, 3297-3305.

41. Kresse, G.; Hafner, J. Ab initio Molecular-Dynamics for Liquid-Metals. *Phys. Rev. B* **1993**, 47, 558-561.

42. Kresse, G.; Furthmüller, J. Efficient Iterative Schemes for Ab Initio Total-Energy Calculations using a Plane-Wave Basis Set. *Phys. Rev. B* **1996**, 54, 11169-11186.

43. Kresse, G.; Furthmüller, J. Efficiency of Ab-Initio Total Energy Calculations for Metals and Semiconductors Using a Plane-Wave Basis Set. *Comput. Mater. Sci.* **1996**, 6, 15-50.

44. Blöchl, P. E. Projector Augmented-Wave Method. *Phys. Rev. B* **1994**, 50, 17953-17979.

45. Kresse, G.; Joubert, D. From Ultrasoft Pseudopotentials to the Projector Augmented-Wave Method. *Phys. Rev. B* **1999**, 59, 1758-1775.

46. Neugebauer, J.; Scheffler, M. Adsorbate-Substrate and Adsorbate-Adsorbate Interactions of Na and K Adlayers on Al(111). *Phys. Rev. B* **1992**, 46, 16067-16080.

47. Meyer, J. A.; Baikie, I. D.; Kopatzki, E.; Behm, R. J. Preferential Island Nucleation at the Elbows of the Au(111) Herringbone Reconstruction Through Place Exchange. *Surf. Sci.* **1996**, 365, L647-L651.

48. Hooper, J.; Kunkel, D. A.; Simpson, S.; Beniwal, S.; Enders, A.; Zurek, E. Chiral surface networks of 3-HPLN — A Molecular Analog of Rounded Triangle Assembly. *Surf. Sci.* **2014**, 629, 65-74.

49. Caffio, M.; Atrei, A.; Bardi, U.; Rovida, G. Growth Mechanism and Structure of Nickel Deposited on Ag(011). *Surf. Sci.* **2005**, 588, 135-148.

50. Trant, A. G.; Jones, T. E.; Gustafson, J.; Noakes, T. C. Q.; Bailey, P.; Baddeley, C. J. Alloy formation in the Au{111}/Ni system - An Investigation with Scanning Tunnelling Microscopy and Medium Energy ion Scattering. *Surf. Sci.* **2009**, 603, 571-579.

51. Colpas, G. J.; Maroney, M. J.; Bagyinka, C.; Kumar, M.; Willis, W. S.; Suib, S. L.; Baidya, N.; Mascharak, P. K. X-Ray Spectroscopic Studies of Nickel-Complexes, with Application to the Structure of Nickel Sites in Hydrogenases. *Inorg. Chem.* **1991**, 30, 920-928.

52. Zubavichus, Y.; Fuchs, O.; Weinhardt, L.; Heske, C.; Umbach, E.; Denlinger, J. D.; Grunze, M. Soft X-Ray-Induced Decomposition of Amino Acids: An XPS, Mass Spectrometry, and NEXAFS Study. *Radiation Research* **2004**, 161, 346-358.

53. Classen, T.; Lingenfelder, M.; Wang, Y.; Chopra, R.; Virojanadara, C.; Starke, U.; Costantini, G.; Fratesi, G.; Fabris, S.; de Gironcoli, S.; Baroni, S.; Haq, S. ; Raval, R.; Kern, K..

Hydrogen and Coordination Bonding Supramolecular Structures of Trimesic Acid on Cu(110). *J. Phys. Chem. A* **2007**, 111, 12589-12603.

54. Barlow, S. M.; Kitching, K. J.; Haq, S.; Richardson, N. V. A Study of Glycine Adsorption on a Cu{110} Surface Using Reflection Absorption Infrared Spectroscopy. *Surf. Sci.* **1998**, 401, 322-335.

55. Barlow, S. M.; Louafi, S.; Le Roux, D.; Williams, J.; Muryn, C.; Haq, S.; Raval, R. Supramolecular Assembly of Strongly Chemisorbed Size-and Shape-Defined Chiral Clusters: S- and R-Alanine on Cu(110). *Langmuir* **2004**, 20, 7171-7176.

56. Hidaka, J.; Shimura, Y. Tris(L-Prolinato)Nickel(II) Complex. *Bull. Chem. Soc. Jpn* **1970**, 43, 2999-3001.

57. Kato, M.; Hayashi, M.; Fujihara, T.; Nagasawa, A. (-)(545)-fac-Delta-Tris(L-prolinato)cobalt(III) trihydrate. *Acta Crystallographica Section E-Structure Reports Online* **2008**, 64, M684-U621.

58. Denning, R.; Piper, T. Optical Activity, Absolute Configuration, and Rearrangement Reactions of Tris Amino Acid Complexes of Cobalt (III) with L-Alanine, L-Leucine, and L-Proline. *Inorg. Chem.* **1966**, 5, 1056-1065.

59. Kong, H. H.; Wang, L. K.; Tan, Q. G.; Zhang, C.; Sun, Q.; Xu, W. Ni-Induced Supramolecular Structural Transformation of Cytosine on Au(111): From One-Dimensional Chains to Zero-Dimensional Clusters. *Chem Commun* **2014**, 50, 3242-3244.

60. Kayushina, R.; Vainshtein, B. Rentgenografiye Opredepenie Strukturi L-Prolina. *Kristallografiya* **1965**, 10, 833-844.

Table of Contents Graphic: